



# Evidence of cathodic peroxydisulfate activation via electrochemical reduction at Fe(II) sites of magnetite-decorated porous carbon: Application to dye degradation in water

S. Mirehbar<sup>a</sup>, S. Fernández-Velayos<sup>a</sup>, E. Mazario<sup>a</sup>, N. Menéndez<sup>a</sup>, P. Herrasti<sup>a</sup>, F.J. Recio<sup>a,\*</sup>, I. Sirés<sup>b,\*</sup>

<sup>a</sup> Departamento de Química Física Aplicada, Facultad de Ciencias, Universidad Autónoma de Madrid, C/Francisco Tomás y Valiente, 7, Cantoblanco, 28049 Madrid, Spain

<sup>b</sup> Laboratori d'Electroquímica dels Materials i del Medi Ambient, Departament de Química Física, Facultat de Química, Universitat de Barcelona, Martí i Franquès 1-11, 08028 Barcelona, Spain

## ARTICLE INFO

### Keywords:

Electrochemical advanced oxidation process  
Methylene Blue  
Persulfate  
Reticulated vitreous carbon  
Sulfate radical

## ABSTRACT

Peroxydisulfate (PDS,  $S_2O_8^{2-}$ )-based advanced oxidation processes have been developed as an alternative to those based on  $\cdot OH$ , as PDS activation yields a much more stable radical like  $SO_4^{\cdot -}$  that can maintain the oxidation ability of water treatment systems for longer time. Here, the electrochemical PDS activation has been investigated using reticulated vitreous carbon (RVC) substrate modified with  $Fe_3O_4$  nanoparticles (NPs) as cathode. The NPs were exhaustively characterized by different surface analysis techniques (TEM, SEM) and Mössbauer spectroscopy. Cyclic voltammetry and linear sweep voltammetry with a rotating disk electrode allowed concluding that the main electrocatalytic role in the cathodic PDS activation to  $SO_4^{\cdot -}$  corresponded to the Fe(II) active sites continuously promoted upon cathodic polarization. These sites were less catalytic for  $O_2$  reduction reaction, although it was still feasible with  $n = 2.7$  electrons as determined from Koutecky-Levich analysis. Both cathodic reactions followed an inner-sphere reaction mechanism. The  $Fe_3O_4$ -modified RVC cathodes were employed to electrolyze Methylene Blue aqueous solutions at pH 3.5, employing different current values and PDS concentrations. Dissolved  $O_2$  was purged to impede the competitive cathodic  $H_2O_2$  production and Fenton's reaction. The occurrence of dye adsorption/electrosorption on the cathode reduced the mass transport limitations, enhancing the reaction between  $SO_4^{\cdot -}$  and organic molecules. The best operation conditions to reach total and fast color removal at 18 min were 2 mM PDS and 10 mA, yielding  $> 80\%$  TOC abatement at 45 min. Reproducible degradation profiles were found after 5 runs, thereby ensuring the stability of the  $Fe_3O_4$ -modified RVC, with no iron sludge production.

## 1. Introduction

In the last few decades, the overgrowth of human population has entailed the massive entry of organic pollutants in all of the environmental compartments, being especially worrisome their accumulation in water because this is an essential ingredient for life. In the present study, Methylene Blue (MB) has been chosen as a model organic pollutant. MB is a fluorescent cationic dye discovered in 1876 [1], with multiple applications nowadays. For example, in medicine it serves for treating illnesses, microbiological staining or intraoperative imaging [1,2], whereas in the textile industry a great surplus of MB is discharged into wastewater effluents due to its poor adhesion to fabrics [3]. Such dye wastewater has become a major environmental issue in countries with intensive dyeing activities, since MB has a high molar absorptivity that causes aesthetic impact and limits the light penetra-

tion into water bodies [4]. Furthermore, the presence of MB in water is reported to cause negative health effects like high blood pressure, nausea, gastrointestinal irritation, skin irritation and abdominal pain [5].

More effective strategies for dye removal from water, not simply implying physical separation but their structural degradation, are thus needed. Outstanding results have been obtained for water and wastewater decontamination by means of advanced oxidation process (AOPs), which are particularly suitable for the degradation of organic pollutants. Classically, the high effectiveness of AOPs has been related to the generation of  $\cdot OH$  onsite [6,7], although the important contribution of  $O_2^{\cdot -}$  and singlet oxygen under some experimental conditions has been increasingly discussed [8]. Lately, AOPs based on the action of sulfate radical anion ( $SO_4^{\cdot -}$ ) have been developed as a viable alternative or complement to  $\cdot OH$ -based AOPs [9,10]. Despite the lower

\* Corresponding authors.

E-mail addresses: [javier.recio@uam.es](mailto:javier.recio@uam.es) (F.J. Recio), [i.sires@ub.edu](mailto:i.sires@ub.edu) (I. Sirés).

<https://doi.org/10.1016/j.jelechem.2021.115807>

Received 8 September 2021; Received in revised form 15 October 2021; Accepted 17 October 2021

Available online 20 October 2021

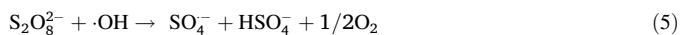
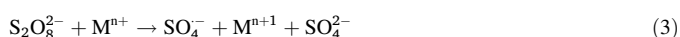
1572-6657/© 2021 The Author(s). Published by Elsevier B.V.

This is an open access article under the CC BY license (<http://creativecommons.org/licenses/by/4.0/>).

redox potential of sulfate radical ( $E^0(\text{SO}_4^{\cdot-}|\text{SO}_4^{2-} = +2.437 \pm 0.019$  vs. SHE  $< E^0(\cdot\text{OH}|\text{H}_2\text{O}) = +2.730 \pm 0.017$  V vs. SHE) [11], its half-life is orders of magnitude longer (30–40  $\mu\text{s}$  vs. 0.02  $\mu\text{s}$ ) [12,13], which makes  $\text{SO}_4^{\cdot-}$  more readily diffused than  $\cdot\text{OH}$ , also evidencing a higher selectivity towards organic matter oxidation. Note, however, that in aqueous matrices both radicals coexist, although  $\text{SO}_4^{\cdot-}$  prevails as main oxidant over  $\cdot\text{OH}$  at pH  $< 7$  [14].

Within this context, electrochemistry has found a niche by giving rise to the so-called electrochemical AOPs [15,16]. The accurate modulation of the electrolysis conditions allows the in-situ electrosynthesis of oxidants like  $\text{H}_2\text{O}_2$  [17–19] and peroxydisulfate (PDS,  $\text{S}_2\text{O}_8^{2-}$ ) [20,21]. These species may act as precursors that can be further activated to yield  $\cdot\text{OH}$  and  $\text{SO}_4^{\cdot-}$ , respectively. The excellent performance of both radicals related to color removal from dye solutions has been widely reported [22–24], as also verified for MB solutions [25].

In electrochemical systems, PDS can be activated through multiple routes: (i) Energy input from ultrasounds, microwaves, UV light or heat, as exemplified in reaction (1) for the thermal activation of persulfate (TAP) that can be accomplished using a water bath [26], a hot plate [27] or a solar thermal equipment [28]; (ii) reaction (2) in the presence of organic molecules (R); (iii) reaction (3) with low valence transition metal ions ( $\text{M}^{n+}$ ) [29–31] such as  $\text{Fe}^{2+}$  [32,33]; and (iv) reactions (4) and (5) with electrogenerated  $\text{H}_2\text{O}_2$  [34] or with its derived homogeneous radical,  $\cdot\text{OH}$ , respectively [34].



In addition to those five routes, the electrochemical activation of persulfate (EAP) is also feasible depending on the electrode materials. For example, reaction (5) could be alternatively mediated by  $\text{M}(\cdot\text{OH})$ , an adsorbed radical formed from water oxidation at the surface of a large  $\text{O}_2$ -overpotential anode M like BDD [17,24] or  $\text{PbO}_2$  [35,36]. The direct anodic oxidation of PDS at the anode surface has also been discussed in the literature, although this is still controversial because some authors suggest that PDS is actually activated to a nonradical transition state that oxidizes water to  $\cdot\text{OH}$  [37,38]. On the other hand, the cathodic route has been much less explored so far [39]. Several scholars hypothesized the direct reduction of PDS at electrocatalytic surfaces via reaction (6) [31], as reported for Pt [40,41], stainless steel [42] and glassy carbon (GC) [43]. Nonetheless, these works do not demonstrate the occurrence of direct electron transfer. On a cathode made of carbon nanotubes, a nonradical PDS activation was observed [44]. In a much more thorough study that included voltammetric measurements and electrolysis in a divided cell, the cathodic PDS reduction to  $\text{SO}_4^{\cdot-}$  was evidenced [45]. In that work, an irreversible reduction peak at Pt and graphite cathodes suggested the occurrence of direct cathodic activation.



Among the different strategies to enhance the electron transfer to/from an electrode in the EAP approach, the use of three-dimensional materials to expose a greater surface area should be seriously considered. Porous carbons like graphite felt and reticulated vitreous carbon are employed as substrates in many electrochemical applications [46,47], and different surface modification procedures allowed enhancing their performance very significantly, as shown by us for the treatment of organic pollutants [35,36,48]. A second finding to take into consideration is the proven effectiveness of the iron-based

materials for PS activation, although the mechanism is still under discussion due to controversy [49]. Magnetite ( $\text{Fe}_3\text{O}_4$ ), which has an inverse spinel cubic structure, has been tested as heterogeneous catalyst in the form of suspended nanoparticles (NPs) in solution for peroxymonosulfate activation [50], whereas PDS has been activated by  $\text{Fe}_3\text{O}_4$ - $\alpha$ - $\text{MnO}_2$  NPs [51] as well as by composites made of  $\text{Fe}_3\text{O}_4$  particles embedded into Camellia seed husk-based biochar that allowed the simultaneous adsorption and catalysis [52]. Some authors also tested the electrochemical degradation of organic pollutants in the presence of suspended  $\text{Fe}_3\text{O}_4$  NPs, aiming to enhance the Fe(III) cathodic reduction [53], although this required a previous adsorption on the catalyst surface.

In this work, PDS electroreduction has been investigated using RVC substrates modified with  $\text{Fe}_3\text{O}_4$  NPs, which have been exhaustively characterized by different surface analysis techniques. The first goal was to discern whether the main electrocatalytic role in PDS activation corresponded to the surface Fe(II) sites continuously promoted upon cathodic polarization, which was assessed by means of cyclic voltammetry and linear polarization on a rotating disk electrode (RDE). At the moment, there exists no strong evidence in the literature on the  $\text{Fe}_3\text{O}_4$ -mediated PDS electroreduction using supported NPs. Afterwards, the  $\text{Fe}_3\text{O}_4$ -modified RVC cathodes were employed to electrolyze MB aqueous solutions at constant applied current ( $I_{\text{app}}$ ) in the presence of different concentrations of PDS, trying to find the best operation conditions for total color removal. The solution TOC was also analyzed during these trials.

## 2. Experimental

### 2.1. Chemical compounds

MB is a heterocyclic aromatic dye with a thiazine structure (see molecular structure in Fig. S1). Its hydrated orm (molecular formula  $\text{C}_{16}\text{H}_{18}\text{ClN}_3\text{S}\cdot\text{H}_2\text{O}$ ,  $> 95\%$  purity, Sigma-Aldrich) was employed. Sodium persulfate ( $\text{Na}_2\text{S}_2\text{O}_8$ ), and sodium sulfate ( $\text{Na}_2\text{SO}_4$ ) of analytical grade were purchased from Panreac. Other solid and liquid chemicals were acquired from Sigma-Aldrich. High purity Milli-Q water with resistivity  $> 18.2 \text{ M}\Omega \text{ cm}$  at  $25^\circ\text{C}$  was used to prepare all the solutions.

### 2.2. Synthesis and characterization of magnetite nanoparticles

$\text{Fe}_3\text{O}_4$  NPs were synthesized using an electrochemical flow reactor operated in recirculation batch mode [54]. Eight iron electrodes were used as cathodes and anodes (area of  $45 \text{ cm}^2$ ). The synthesis was carried out for 1 h at a constant  $I_{\text{app}} = 0.7 \text{ A}$  in a 40 mM NaCl solution. The obtained NPs were separated magnetically as they were formed, being further rinsed with Milli-Q water several times until the supernatant was colorless. This simple and economic methodology allowed obtaining an estimated yield of 1 g NPs per hour.

The synthesized NPs were dried under vacuum overnight and their morphology was analyzed by transmission electron microscopy (TEM) using a JEOL JEM 1010 microscope operated at 100 kV. The average size of the NPs were determined upon measurement of at least 100 particles. The iron composition was determined by Mössbauer spectroscopy. Mössbauer spectra were recorded at room temperature in triangular mode using an emission spectrometer equipped with a  $^{57}\text{Co}/\text{Rh}$  source. The spectral analyses were performed via a non-linear adjustment, using the NORMOS program [55], and energy calibrations were accomplished with an  $\alpha$ -Fe foil (6  $\mu\text{m}$ ).

### 2.3. Preparation and characterization of $\text{Fe}_3\text{O}_4$ -modified RVC electrodes

RVC foam (45 ppi, ULTRAMET) was modified with the synthesized  $\text{Fe}_3\text{O}_4$  NPs following a dip coating procedure. The RVC pieces were

perfectly cut into dimensions of 70 mm × 20 mm × 10 mm (reproducible bare electrode mass of  $1.8 \pm 0.4$  g, and volumetric surface area of  $30 \text{ cm}^{-1}$ ). The pieces were subsequently washed with acetone and water, and then entirely submerged into a colloidal suspension of  $\text{Fe}_3\text{O}_4$  NPs ( $10 \text{ g L}^{-1}$ ) for 30 min under sonication, employing a Bandelin ultrasonic bath DT 100H Sonorex Digitec (maximum power of 320 W) with heating. The obtained electrodes were washed with Milli-Q water and dried at  $60^\circ\text{C}$  for 12 h. The mass of deposited NPs was practically constant ( $60 \pm 5 \text{ mg}$ ).

The morphologies of bare and modified RVC electrodes were characterized by scanning electron microscopy (SEM) using a Hitachi S-3000 N microscope. The equipment offered a resolution of 3 nm at 25 kV and a tension range of 0.3 to 30 kV with an environmental secondary electron detector (ESED) coupled to an Oxford Instruments energy dispersive X-ray analyzer (model INCA x-sight).

#### 2.4. Electrochemical characterization and bulk electrolytic trials

The electrochemical measurements were conducted on a GC RDE (geometrical area of  $0.196 \text{ cm}^2$ ) from PINE Instruments as working electrode, since it is considered a valid model surface to obtain data comparable with RVC. In most cases, the GC was further modified with an ink made of  $\text{Fe}_3\text{O}_4$  NPs and Vulcan XC-72 carbon black, which was prepared by thoroughly mixing 2 mg of NPs and 2 mg of carbon and further hand-milling with an agate mortar. The resulting powder was dispersed through sonication (same aforementioned bath) in a beaker containing 1 mL of isopropanol and 4 mL of Milli-Q water. Then, 20  $\mu\text{L}$  of Nafion (5 wt% in alcohol, Sigma-Aldrich) were added and the mixture was sonicated for 30 min to ensure its homogeneity. The NPs concentration in the inks was set to  $\sim 0.5 \text{ mg mL}^{-1}$ . The GC electrode surface was modified by dropping 20  $\mu\text{L}$  of the ink and then dried under  $\text{N}_2$  flow.

The electrochemical tests were carried out with an Autolab PGSTAT302N potentiostat/galvanostat (Metrohm) controlled with Nova 2.0 software. A conventional three-electrode cell that contained a bare or modified GC RDE as working electrode, as well as an Ag|AgCl (saturated KCl) and a graphite rod as reference and counter electrode, respectively, was used. All the potentials in this work are referred to the reversible hydrogen electrode (RHE) under standard conditions, which agrees with the following expression:  $E(\text{RHE}) = E(\text{Ag}|\text{AgCl}(\text{sat. KCl})) + 0.190 + 0.059\text{pH}$ . The electrochemical characterization was conducted by cyclic voltammetry in an  $\text{N}_2$ -saturated supporting electrolyte (0.1 M  $\text{Na}_2\text{SO}_4$  solution prepared in Milli-Q water and adjusted to pH 3.5 with  $\text{H}_2\text{SO}_4$ ). The oxygen reduction reaction (ORR) tests were performed by linear polarization in the same supporting electrolyte but saturated with  $\text{O}_2$ , at different rotation rates ( $\omega$ ), and the number of electrons was determined from the Koutecky-Levich equation [56]. The persulfate reduction was investigated in an  $\text{O}_2$ - or  $\text{N}_2$ -saturated electrolyte solution in the presence of 2 mM PDS, at  $\omega = 1600 \text{ rpm}$ . All voltammograms were recorded at a scan rate ( $V$ ) of  $5 \text{ mV s}^{-1}$ .

The degradation experiments were performed in batch using an undivided glass reactor (120 mm in height × 60 mm in diameter). Mechanical stirring with PTFE blade impellers at 650 rpm was applied in all the experiments to ensure good mixing. A constant  $\text{N}_2$  flow was always fed to the solutions in order to avoid the ORR contribution. Bare or  $\text{Fe}_3\text{O}_4$ -modified RVC (dimensions of 50 mm × 20 mm × 10 mm corresponded to the immersed part) were used as the cathode and graphite rod (70 mm in length × 6 mm in diameter) as the anode. To ensure the electric contact between the working electrode and the potentiostat, a graphite rod was fixed to the RVC piece with silver conductive paint. The electrodes were connected to the aforementioned potentiostat/galvanostat, which supplied constant  $I$  of 5–15 mA in DC mode. The bulk electrolyses were performed with solutions of 200 mL containing 50  $\text{mg L}^{-1}$  MB (i.e., 0.15 mM MB, total organic carbon (TOC) =  $30 \text{ mg L}^{-1}$ ) and 50 mM

$\text{Na}_2\text{SO}_4$  at pH 3.5. When needed, sodium persulfate was added to the MB solution just before supplying  $I$ , at a concentration of 1–6 mM.

The absorbance decay of the MB solutions was determined by UV/Vis spectroscopy on a Perkin-Elmer LAMBDA 35 UV/Vis spectrophotometer set at  $\lambda_{\text{max}} = 663 \text{ nm}$  (see UV/Vis spectrum in Fig. S1). The solution decolorization has been expressed as follows [32]:

$$\% \text{Color Removal} = \frac{A_0 - A_t}{A_0} \times 100 \quad (7)$$

where  $A_0$  and  $A_t$  account for the solution absorbance at 0 min and at time  $t$ . Some reuse tests were comparatively performed by submerging the cathode in milli-Q water for 1 h after stopping the current supplied for the dye treatment. The solution TOC was analyzed at selected time intervals employing a TOC analyzer from Shimadzu (model VCSH).

### 3. Results and discussion

#### 3.1. Characterization of $\text{Fe}_3\text{O}_4$ nanoparticles and RVC electrodes

The morphology of the  $\text{Fe}_3\text{O}_4$  NPs synthesized in an electrochemical flow cell as explained in subsection 2.2 is shown in Fig. 1a, evidencing a quasi-spherical shape with a certain degree of aggregation. A mean diameter of  $21 \pm 7 \text{ nm}$  has been determined by measuring this value from at least 100 particles observed in the different micrographs acquired. The standard deviation value informs about a moderate polydispersity of the NPs produced in recirculation mode. The Mössbauer spectrum of the synthesized NPs at 300 K can be observed in Fig. 1b. A typical hyperfine pattern consisting of two overlapping six-line magnetic subspectra is depicted, yielding the following hyperfine parameters:  $IS = 0.556(4) \text{ mm s}^{-1}$  and the magnetic hyperfine field  $H = 44.64(4) \text{ T}$  assignable to  $^{57}\text{Fe}$  in the tetrahedral position; and  $IS = 0.329(2) \text{ mm s}^{-1}$  and  $H = 48.50(1) \text{ T}$  related to the octahedral sites of the spinel lattice. The magnetic hyperfine values are slightly inferior to the ones corresponding to magnetite bulk material, but similar to reported values of  $\text{Fe}_3\text{O}_4$  NPs with a diameter of 19 nm [57], thereby confirming the predominant magnetite structure in the electrochemically synthesized sample.

Before modifying the RVC substrate with the  $\text{Fe}_3\text{O}_4$  NPs just characterized, the morphology of the bare RVC (45 ppi) was observed by SEM. Fig. 1c shows a pore size of about 500–600  $\mu\text{m}$ , in good agreement with the porosity value provided by the manufacturer. SEM also served to corroborate the efficient deposition and homogeneous distribution of the particles. The surface analysis of the  $\text{Fe}_3\text{O}_4$ -modified RVC (Fig. 1d) allows confirming that 30 min of dip coating is a suitable duration to obtain a sufficiently uniform coating of the substrate. It is evident that the coating is rough and the NPs are well distributed throughout the surface.

#### 3.2. Electrochemical activation of PDS

A GC RDE, either bare or modified with the  $\text{Fe}_3\text{O}_4$  NPs, was employed as the working electrode in a three-electrode cell to carry out these tests. The electrochemical characterization of the  $\text{Fe}_3\text{O}_4$  NPs was first performed by cyclic voltammetry in an  $\text{N}_2$ -saturated 0.1 M  $\text{Na}_2\text{SO}_4$  solution at pH 3.5. Fig. 2a shows the voltammogram obtained with the  $\text{Fe}_3\text{O}_4$ -modified GC RDE, which presents an electrochemically irreversible Faradaic process that can be related to the Fe (III)/Fe(II) redox process on the NPs surface. The anodic and cathodic peak potentials appear at 0.79 and 0.31 V vs. RHE, respectively. Note that a similar irreversible behavior has been reported for magnetite and ferrite NPs in acid media [58]. The cathodic process can be represented as follows:



where  $\equiv$  represents the solid state.



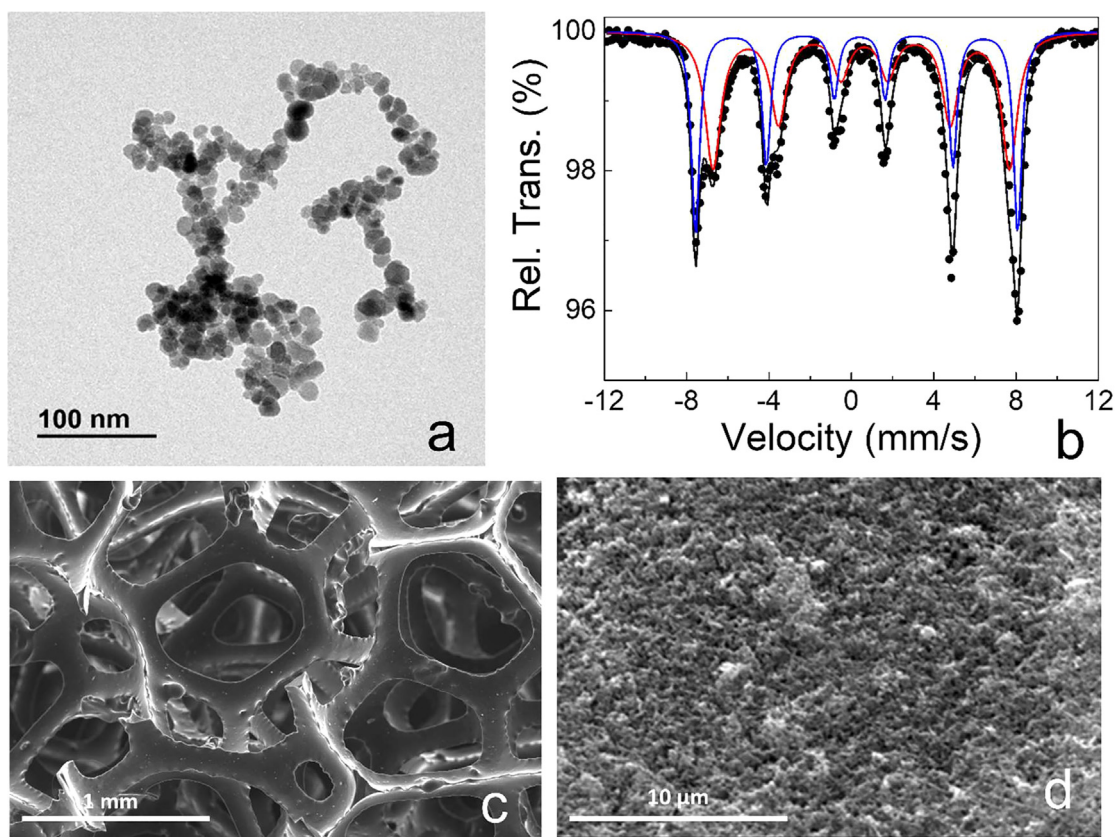
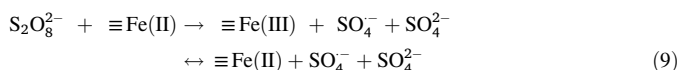


**Fig. 1.** (a) TEM micrograph of  $\text{Fe}_3\text{O}_4$  NPs synthesized in a 40 mM NaCl solution using an electrochemical flow cell, equipped with iron electrodes, for 1 h at  $I_{\text{app}} = 0.7$  A. (b) Room temperature Mössbauer spectrum of the as-synthesized  $\text{Fe}_3\text{O}_4$  NPs. (c) SEM image of bare RVC substrate (45 ppi). (d) SEM image of  $\text{Fe}_3\text{O}_4$ -modified RVC.

The electrocatalytic activity of the  $\text{Fe}_3\text{O}_4$  NPs has been further studied in terms of promotion and/or enhancement of both, PDS and  $\text{O}_2$  reduction reactions. In particular, in PDS-based AOPs the ORR can become a relevant simultaneous phenomenon during the degradation of organic pollutants, since it can favor the occurrence of heterogeneous electro-Fenton (EF) process as dissolved  $\text{O}_2$  may yield  $\text{H}_2\text{O}_2$  as Fenton's reactant in the presence of adsorbed  $\text{Fe}_3\text{O}_4$  NPs [15,17,19]. As can be observed in Fig. 2a, a comparison between the polarization curves with bare and  $\text{Fe}_3\text{O}_4$ -modified GC allows concluding that the NPs are active for both reduction reactions. This is readily deduced from the clear decrease in the onset potential for both reactions using the modified working electrode. An additional and very remarkable finding, as evidenced by comparing both reduction signals using the same modified electrode, is the greater electroactivity of  $\text{Fe}_3\text{O}_4$  towards PDS reduction. The corresponding onset potential was 0.150 V more positive as compared to the ORR. Furthermore, the onset potential for each reaction appears in the region related to the cathodic process assigned to the  $\text{Fe(III)}$  to  $\text{Fe(II)}$  conversion previously observed in the cyclic voltammogram (reaction (8)). Therefore, this is an evidence of cathodic  $\text{O}_2$  reduction and PDS activation (reaction (9), 1st step) mediated by electrogenerated  $\text{Fe(II)}$  sites. The latter process mimics the more commonly reported PDS activation in solution (reaction (3)) [32]; however, in solution reaction there is a gradual accumulation of  $\text{Fe}^{3+}$ , whereas with the immobilized NPs the cathodic polarization becomes essential because it ensures that the iron centers remain continuously available as  $\text{Fe(II)}$ , as illustrated in the equilibrium shown in reaction (9) (2nd step).



The occurrence of reaction (9) at  $\text{Fe}_3\text{O}_4$  surface sites is potentially advantageous, since it avoids the need of dissolved metal cations like  $\text{Fe}^{2+}$  that tend to precipitate in aqueous solution if the pH is not sufficiently acid. Hence, the absence of iron sludge production directly reduces the cost and time associated to its management.

The direct connection found between the  $\text{Fe(III)}/\text{Fe(II)}$  redox potential and the onset potential for both reactions mentioned above implies an inner-sphere reaction mechanism, as previously proposed for the ORR catalyzed by ferrite NPs, iron-doped carbon materials and single atom molecular catalysts [59–61]. From this, it can be assured that  $\text{O}_2$  and PDS must be adsorbed on the  $\text{Fe(II)}$  sites to start the electroreduction. The PDS reduction reaction presented diffusional control at low overpotentials (0.2 V vs. RHE, Fig. 2a); this phenomenon also occurred during the ORR, although at much greater overpotentials (-0.4 V vs. RHE, Fig. S2a) and attaining current values one order of magnitude higher as compared to PDS (not shown). The total number of electrons for the ORR has been determined via Koutecky-Levich analysis of data obtained from linear sweep voltammeteries recorded at different rotation rates (Fig. S2a,b). The results highlight a mixed mechanism via 2.7 electrons, informing about the production of  $\text{H}_2\text{O}_2$  as main product that could be further employed to stimulate Fenton's reaction during the treatment of aerated contaminated solutions.

Based on the latter finding, the presence of dissolved  $\text{O}_2$  in aerated water effluents to be treated by PDS-based AOPs can lead to an overestimation of the oxidizing role of  $\text{SO}_4^{\cdot-}$ , since  $\text{H}_2\text{O}_2$  not only induces Fenton's reaction either with dissolved  $\text{Fe}^{2+}$  or anchored  $\text{Fe(II)}$  [15,62], but it also acts as PDS activator via reaction (4). In such scenario, the degradation of the organic molecules is expected to be caused by the combined action of both,  $\text{SO}_4^{\cdot-}$  and  $\cdot\text{OH}$  [34,63]. Aiming

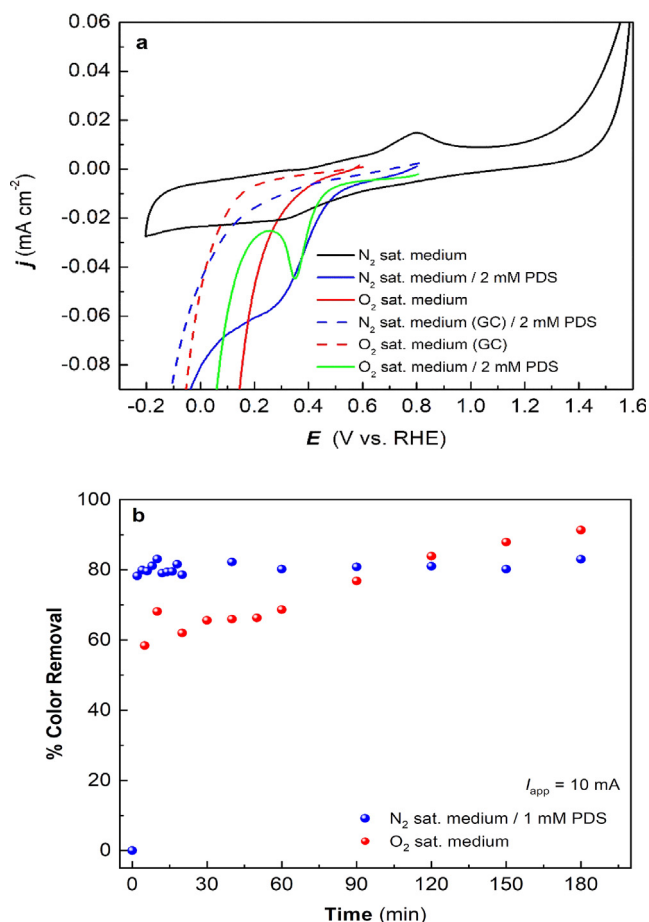


**Fig. 2.** (a) Cyclic voltammetry (—) in  $N_2$ -saturated medium using a glassy carbon (GC) RDE coated with an ink made of  $Fe_3O_4$  NPs + Vulcan XC-72 carbon black as working electrode, recorded at  $v = 5$  mV s<sup>-1</sup> without rotation. Linear sweep voltammeteries in the same medium, with 2 mM PDS, using the same working electrode (—) or an unmodified GC RDE (---). Linear sweep voltammeteries in  $O_2$ -saturated medium, without PDS, using the modified (—) or the unmodified GC RDE (---) as working electrode. Linear sweep voltammetry in  $O_2$ -saturated medium, with 2 mM PDS, using the modified GC RDE (—). All linear sweep voltammograms were recorded at  $v = 5$  mV s<sup>-1</sup> and  $\omega = 1600$  rpm, using a three-electrode cell containing a 0.1 M  $Na_2SO_4$  solution at pH 3.5, with an Ag|AgCl (sat. KCl) and a graphite rod as reference and counter electrodes. (b) Percentage of color removal vs. time during the treatment of 200 mL of solutions containing 50 mg L<sup>-1</sup> (0.15 mM) MB and 50 mM  $Na_2SO_4$  at pH 3.5, at constant  $I_{app} = 10$  mA using an undivided glass reactor equipped with an  $Fe_3O_4$ -modified RVC piece and a graphite rod as the cathode and anode, respectively. One trial was made in an  $N_2$ -saturated solution in the presence of 1 mM PDS, whereas the other one was made without PDS in an  $O_2$ -saturated solution.

to evaluate the influence of  $O_2$ , solutions containing 50 mg L<sup>-1</sup> (0.15 mM) MB and 50 mM  $Na_2SO_4$  at pH 3.5 were electrolyzed at  $I_{app} = 10$  mA using an undivided reactor with an  $Fe_3O_4$ -modified RVC cathode and a graphite anode. The PDS-based process (i.e.,  $SO_4^{\cdot-}$  as main oxidant) was tested upon addition of 1 mM PDS to the  $N_2$ -saturated solution, whereas the heterogeneous EF process (i.e.,  $\cdot OH$  as main oxidant) was performed under  $O_2$  saturation without PDS. As highlighted in Fig. 2b, a high percentage of color removal was attained after 180 min by both treatments, being superior in the  $\cdot OH$ -mediated process (90% vs. 80%) thanks to the greater redox potential of this radical as compared to  $SO_4^{\cdot-}$ . Nonetheless, the PDS-based treatment was comparatively more effective within the first minutes, as the maximum decolorization of 80% with PDS was already achieved at 2 min, a value significantly higher than 60% reached by

EF. The slower initial MB degradation in the latter process can be accounted for by the absence of the  $\cdot OH$  precursor in the initial solution, since  $H_2O_2$  must be electrogenerated on site, in contrast to the PDS process in which a fast activation to  $SO_4^{\cdot-}$  is feasible from the beginning. Once a sufficiently high  $H_2O_2$  concentration was accumulated ( $\sim 90$  min), the EF process became superior.

Additionally, note that in heterogeneous EF process, the Fe(II) active sites present on the deposited NPs surface are needed to catalyze two reactions to finally produce the  $\cdot OH$ : the 2-electron ORR and the heterogeneous Fenton's reaction. Conversely, in the PDS-based AOP all the catalytic sites are available for  $SO_4^{\cdot-}$  generation without requiring any intermediate whose formation could decelerate the degradation. From the trends of Fig. 2b, it can then be concluded that even the decolorization of aerated solutions can be readily promoted by PDS alone, being the contribution of  $\cdot OH$  less relevant, although this radical can become useful as the electrolysis is prolonged in order to reach a large percentage of TOC decay.

### 3.3. Focus on PDS-based advanced oxidation treatment of dye solutions

Iron-based NPs and hybrid materials have been successfully employed in water decontamination promoted by the adsorption and magnetic separation of the organic pollutants [64–68]. To discern whether the adsorption and electrosorption of MB on the modified RVC cathode plays a significant role in the degradation process,  $N_2$ -saturated solutions containing 50 mg L<sup>-1</sup> MB and 50 mM  $Na_2SO_4$  at pH 3.5 without PDS were treated using the same reactor and electrodes described in the previous subsection. The effect of  $I_{app}$  on the percentage of color removal over time is depicted in Fig. 3a. The MB removal via purely physical adsorption (i.e., no applied current) upon contact of the stirred solution with the large surface area RVC cathode was negligible, reaching an average value as low as 3%. This behavior is attributed to the electrostatic repulsion between the MB and the surface of the  $Fe_3O_4$  NPs; the isoelectric point of the particles ( $pI \sim 6.5$ ) induced the appearance of a positive surface charge at pH 3.5, whereas at such solution pH the MB ( $pK_a = 3.8$ ) was mainly protonated [64,69]. Note that Hung et al. [70] also reported that MB is believed to become adsorbed onto the surface of  $Fe_3O_4$  NPs, which they employed as catalyst in non-electrochemical experiments.

The situation changed upon galvanostatic electrolysis, which induced an electroadsorption phenomenon that contributed to reach a certain degree of decolorization at all  $I_{app}$  tested. At 6 min, the color removal was 2%, 8%, 28% and 14% operating at 0, 5, 10 and 15 mA, respectively. The detrimental effect of current increase from 10 to 15 mA can be explained by a more ordered adsorption of the MB molecules onto the NPs and uncoated RVC, both on the surface and through the pores, at 10 mA; a higher cathodic current causes a faster migration of MB in its cationic form, facilitating a less ordered surface coverage that potentially blocks some of the pores during the first minutes. At 30 min, even at 10 mA the cathode coverage tended to reach a limit and hence, the percentage of color removal became similar (plateau around 37%–40%) at the two highest  $I_{app}$  values, being twice greater than that at 5 mA (18%).

To corroborate that the color loss evidenced in Fig. 3a was due to adsorption/electrosorption on the  $Fe_3O_4$ -modified RVC piece and not to transformation phenomena, a desorption test was performed at the end of the experiments at each  $I_{app}$  by immersing the cathode into Milli-Q water for 60 min under vigorous stirring. The TOC content of final solutions obtained from the treatment of MB solutions and from desorption trials was determined, as shown in Fig. 3b. It is evident that the concentration of organic carbon in the system remained constant regardless of the  $I_{app}$  value, which means that no mineralization occurred. However, the distribution of this TOC differed in each treatment, with maximum decay of dissolved TOC found at 10–15 mA, in agreement with maximum color removal under these conditions (Fig. 3a). From a practical point of view, the existence of adsorption

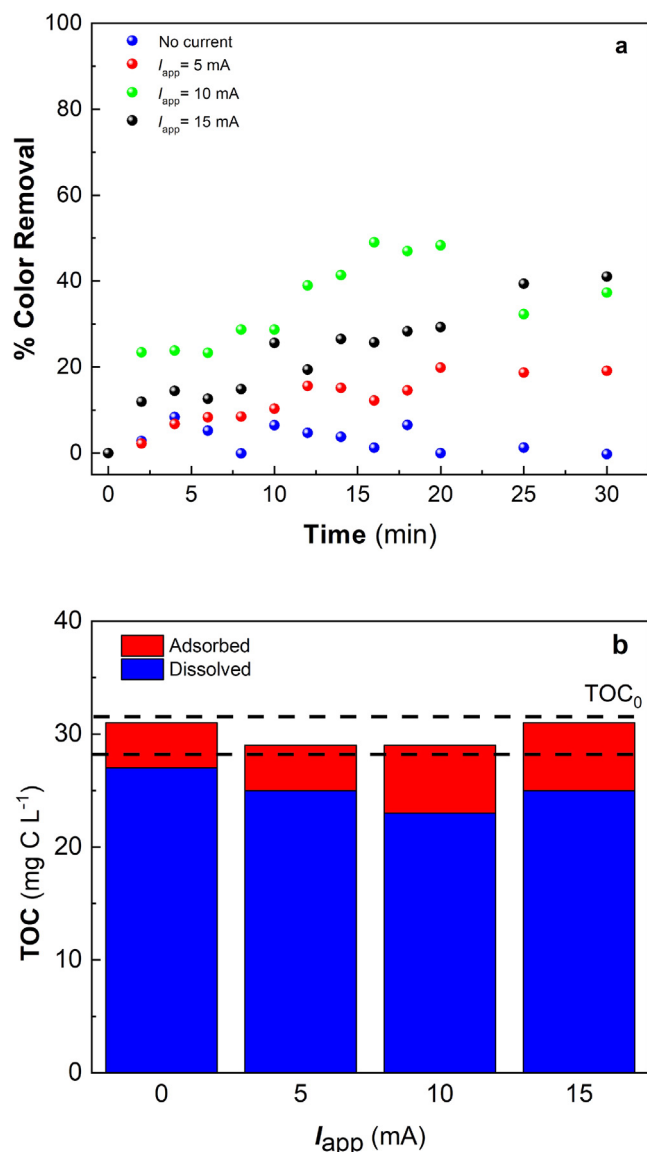


**Fig. 3.** (a) Effect of  $I_{app}$  on the percentage of color removal over time during the treatment of 200 mL of  $N_2$ -saturated solutions containing 50 mg L<sup>-1</sup> (0.15 mM) MB and 50 mM  $Na_2SO_4$  at pH 3.5 using the same reactor and electrodes described in Fig. 2. (b) Dissolved TOC content at the end of the four trials. The difference between these values and  $TOC_0$  accounts for the organic carbon adsorbed throughout the tests.

phenomena is expected to be beneficial because the MB oxidation and mineralization will be accelerated thanks to the minimization of mass transport limitations.

A critical parameter in PDS-based AOPs is the PDS concentration, as this is the direct source of  $SO_4^{\cdot-}$ .  $N_2$ -saturated MB solutions as those mentioned for tests in Fig. 3 but containing 1–6 mM PDS were electrolyzed at  $I_{app} = 10$  mA, using the same reactor and electrodes. Fig. 4a illustrates an abrupt color decay at the beginning of all the experiments, whereupon the decolorization percentages stabilized until the end of the electrolysis. A minimum of 2 mM PDS was needed to gradually achieve 100% color removal, since the use of 1 mM PDS only allowed 80% (Fig. 2b). When a much greater reagent concentration of 6 mM was employed, a quicker total decolorization occurred at 2 min instead of 18 min, which suggests that the  $Fe_3O_4$  NPs surface always contains a sufficiently high accessibility to Fe(II) sites to accelerate the production of  $SO_4^{\cdot-}$  if enough PDS is fed to the cathode. How-

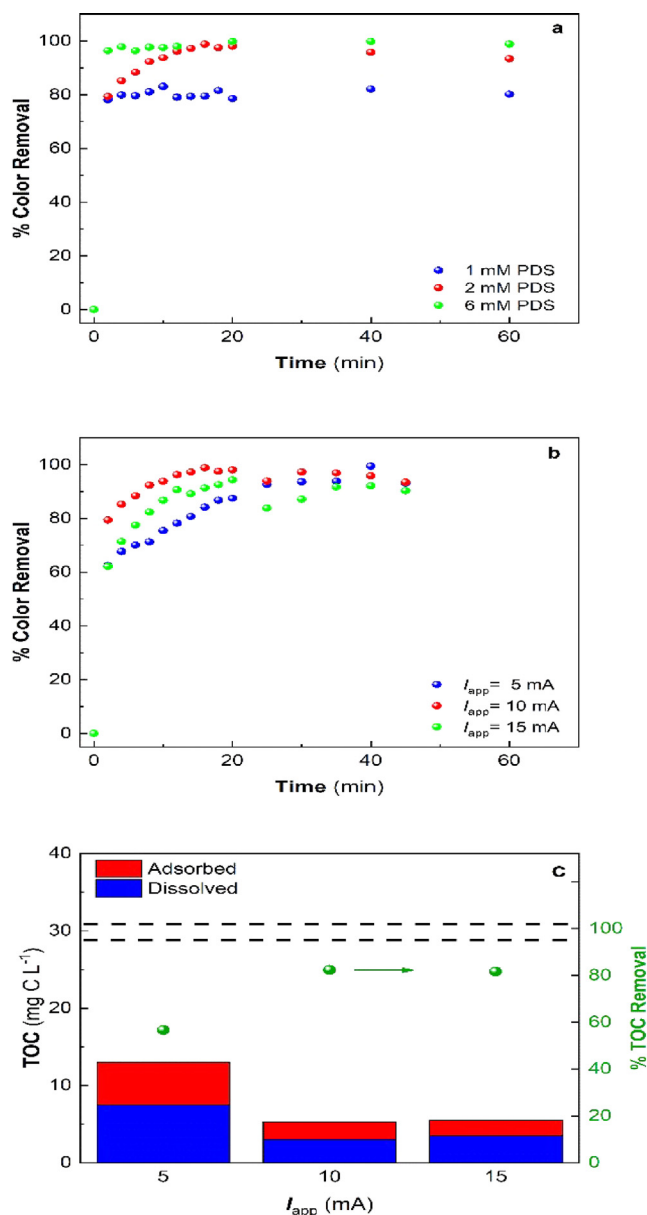


**Fig. 4.** (a) Effect of PDS concentration on the time course of the percentage of color removal during the treatment of 200 mL of dye solutions analogous to those described in Fig. 3 at  $I_{app} = 10$  mA, using the same reactor and electrodes. (b) Effect of  $I_{app}$  under the conditions of plot (a) at 2 mM PDS. (c) Dissolved TOC content at the end of the trials of plot (b), accounting for the percentage of TOC removal depicted on the right y-axis. The difference between these values and  $TOC_0$  corresponds to the organic carbon adsorbed throughout the tests.

ever, it was also observed that such high PDS content became detrimental in terms of cathode durability, since the solution turbidity underwent an evident increase during the test with 6 mM PDS. After the test, clear damage of the modified RVC electrode was detected, entailing a decrease in its dimensions and a greater embrittlement that put its mechanical stability at risk. The degradation of the material could be associated with the high amount of  $SO_4^{\cdot-}$  generated at the cathode surface, which induced the oxidation of the carbon.

Considering a balanced performance integrating both, solution decontamination and electrode stability, the effect of  $I_{app}$  was investigated under the conditions of Fig. 4a at 2 mM PDS. In Fig. 4b, it can be seen that the lowest  $I_{app} = 5$  mA was able to yield complete color



removal after 40 min in a gradual manner. The much slower degradation as compared to the test made at 10 mA (18 min) is mainly justified by the more limited regeneration of the Fe(II) active sites, which eventually decelerates the production of  $\text{SO}_4^{\cdot-}$ . Worth commenting, a preliminary test made with no current supply revealed a substantial tendency of MB to precipitate over time due to the action of PDS, which consequently led to the loss of PDS in the medium [71]. An increase of  $I_{\text{app}}$  to 15 mA did not yield further amelioration, only reaching a maximum color loss of 90–95%, maybe because an excessive production of  $\text{SO}_4^{\cdot-}$  enhanced their self-decomposition through radical–radical reactions (see below). On the other hand, despite the similarities in the decolorization profiles, much clearer differences appeared during TOC analysis ( $\text{TOC}_0 \sim 30 \text{ mg L}^{-1}$ ). Fig. 4c presents the dissolved (direct measurement) and adsorbed (obtained upon desorption, see Fig. 3) TOC values after 45 min of each treatment shown in Fig. 4b, along with the corresponding TOC abatement percentage (i.e., TOC escaping the system upon mineralization). The electrolysis carried out at 5 mA allowed decreasing the TOC in solution to  $\sim 7.5 \text{ mg L}^{-1}$ , with the organic matter adsorbed on the cathode accounting for  $\sim 5 \text{ mg L}^{-1}$  TOC, which means that 58% of  $\text{TOC}_0$  was effectively removed (i.e., mineralized to  $\text{CO}_2$ ). The TOC abatement was greater ( $\sim 83\%$ ) at the two highest  $I_{\text{app}}$  values, whose effect was similar and yielded final TOC values of  $\sim 3$  and  $\sim 2 \text{ mg L}^{-1}$  in solution and on RVC, respectively. It is interesting to highlight that, although at

15 mA the color removal was lower than that at 5 mA, its ability to promote the gradual degradation of the reaction byproducts was larger. It can then be inferred that at 15 mA, the excess of  $\text{SO}_4^{\cdot-}$  mainly participated in the oxidation of byproducts.

Finally, in order to evaluate the reusability of a freshly prepared  $\text{Fe}_3\text{O}_4$ -modified RVC cathode, five consecutive degradation runs were performed under the conditions described in Fig. 4, at 2 mM PDS and  $I_{\text{app}} = 10 \text{ mA}$ . Fig. 5a illustrates the percentage of color removal over time during the tests, evidencing a complete decolorization at 18 min in all cases, although in the 5th run the profile was slightly different and suggested a slower degradation that can be related to performance loss. The excellent behavior of the system after the 5 runs was further corroborated from TOC analysis. Quite reproducible dissolved and adsorbed TOC values were determined after each reuse under study (Fig. 5b), always accounting for  $>80\%$  of mineralization.

#### 4. Conclusions

This work demonstrates that the substantial enrichment of magnetite surface with Fe(II) sites during its cathodic polarization leads to the enhanced electrocatalysis of PDS and  $\text{O}_2$  reduction as compared to bare carbon cathode. The  $\text{Fe}_3\text{O}_4$  activity towards PDS activation was comparatively greater than that towards  $\text{O}_2$ . The heterogeneous conversion of PDS into  $\text{SO}_4^{\cdot-}$  mimics the more conventional PDS activation by dissolved  $\text{Fe}^{2+}$ . This is clearly advantageous for practical application, since the sludge production typically associated to the precipitation of dissolved metal cations like  $\text{Fe}^{2+}$  and  $\text{Fe}^{3+}$  can be impeded. The viability of PDS-based treatments to degrade an organic molecule like MB dye in  $\text{N}_2$ -saturated medium has been proven, achieving a complete decolorization of solutions in short time upon optimization of the electrolysis conditions. TOC abatements  $>80\%$  were also attained after relatively short treatments. PDS concentration must not be too high or too low, since the electrode stability is compromised or the amount of  $\text{SO}_4^{\cdot-}$  is insufficient, respectively. Further work should address the simultaneous heterogeneous EF process using dissolved  $\text{O}_2$ .

#### CRediT authorship contribution statement

**S. Mirehbar:** Investigation, Methodology, Validation. **S. Fernández-Velayos:** Investigation, Methodology. **E. Mazario:** Data curation, Formal analysis, Writing – review & editing. **N. Menéndez:** Funding acquisition, Project administration, Resources. **P. Herrasti:** Funding acquisition, Project administration, Resources, Writing – review & editing. **F.J. Recio:** Conceptualization, Formal analysis, Data curation, Supervision, Writing – original draft, Writing – review & editing. **I. Sirés:** Conceptualization, Formal analysis, Data curation, Supervision, Writing – original draft, Writing – review & editing.

#### Declaration of Competing Interest

The authors declare that they have no known competing financial interests or personal relationships that could have appeared to influence the work reported in this paper.

#### Acknowledgments

The authors kindly acknowledge financial support from projects PGC2018-095642-B-I00 (MINECO, Spain) and PID2019-109291RB-I00 (MCIN/AEI/10.13039/501100011033, Spain). E. M. is grateful to the Madrid Government (Comunidad de Madrid, Spain) under the Multiannual Agreement with Universidad Autónoma de Madrid to encourage young research doctors within the context of the V PRICIT (Regional Program of Research and Technological Innovation, reference SI1-PJI-2019-00366).

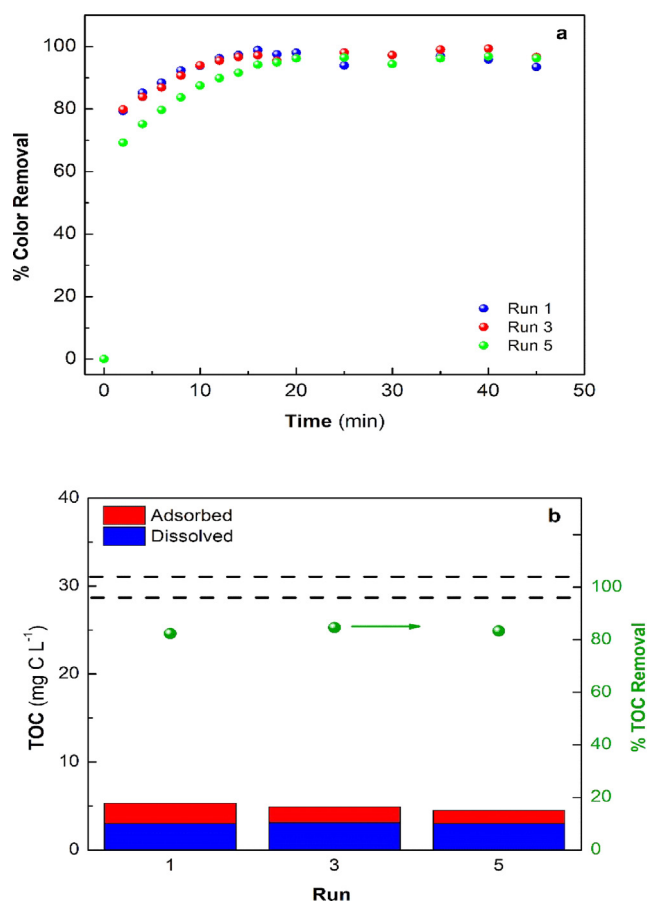


**Fig. 5.** (a) Time course of the percentage of color removal during the treatment of 200 mL of dye solutions analogous to those described in Fig. 4 at 2 mM PDS and  $I_{\text{app}} = 10 \text{ mA}$ , using the same reactor and a freshly prepared  $\text{Fe}_3\text{O}_4$ -modified RVC cathode reused for five consecutive runs (45 min each). (b) Dissolved TOC content (left y-axis) and percentage of TOC removal (right y-axis) at the end of the trials of plot (a). The difference between the former values and  $\text{TOC}_0$  corresponds to the organic carbon adsorbed throughout the tests.

## Appendix A. Supplementary data

Supplementary data to this article can be found online at <https://doi.org/10.1016/j.jelechem.2021.115807>.

## References

- [1] T. Cwalinski, W. Polom, L. Marano, G. Roviello, A. D'Angelo, N. Cwalina, M. Matuszewski, F. Roviello, J. Jaskiewicz, K. Polom, Methylene Blue—Current knowledge, fluorescent properties, and its future use, *J. Clin. Med.* 9 (11) (2020) 3538, <https://doi.org/10.3390/jcm9113538>.
- [2] C. Ponraj, V. G., J. Daniel, A review on the visible light active BiFeO<sub>3</sub> nanostructures as suitable photocatalyst in the degradation of different textile dyes, *Environ. Nanotechnol. Monit. Manage.* 7 (2017) 110–120, <https://doi.org/10.1016/j.enmm.2017.02.001>.
- [3] A.M. Kossawattarachchi, T.R. Cook, Repurposing the industrial dye Methylene Blue as an active component for redox flow batteries, *ChemElectroChem* 5 (22) (2018) 3437–3442, <https://doi.org/10.1002/celec.v5.2210.1002/celec.201801097>.
- [4] F.A. Ozdemir, B. Demirata, R. Apak, Adsorptive removal of methylene blue from simulated dyeing wastewater with melamine-formaldehyde-urea resin, *J. Appl. Polym. Sci.* 112 (6) (2009) 3442–3448, <https://doi.org/10.1002/app.v112:610.1002/app.29835>.
- [5] H. Lyu, B. Gao, F. He, A.R. Zimmerman, C. Ding, J. Tang, J.C. Crittenden, Experimental and modeling investigations of ball-milled biochar for the removal of aqueous methylene blue, *Chem. Eng. J.* 335 (2018) 110–119, <https://doi.org/10.1016/j.cej.2017.10.130>.
- [6] M.A. Oturan, J.-J. Aaron, Advanced oxidation processes in water/wastewater treatment: Principles and applications. A review, *Crit. Rev. Environ. Sci. Technol.* 44 (23) (2014) 2577–2641, <https://doi.org/10.1080/10643389.2013.829765>.
- [7] D.B. Miklos, C. Remy, M. Jekel, K.G. Linden, J.E. Drewes, U. Hübner, Evaluation of advanced oxidation processes for water and wastewater treatment — A critical review, *Water Res.* 139 (2018) 118–131, <https://doi.org/10.1016/j.watres.2018.03.042>.
- [8] J. Al-Nu'airat, I. Oluwoye, N. Zeinali, M. Altarawneh, B.Z. Dlugogorski, Review of chemical reactivity of singlet oxygen with organic fuels and contaminants, *Chem. Rec.* 21 (2) (2021) 315–342, <https://doi.org/10.1002/tcr.v21.210.1002/tcr.202000143>.
- [9] X. Duan, S. Yang, S. Wacławek, G. Fang, R. Xiao, D.D. Dionysiou, Limitations and prospects of sulfate-radical based advanced oxidation processes, *J. Environ. Chem. Eng.* 8 (4) (2020) 103849, <https://doi.org/10.1016/j.jece.2020.103849>.
- [10] Z.-Y. Guo, C.-X. Li, M. Gao, X. Han, Y.-J. Zhang, W.-J. Zhang, W.-W. Li, Mn-O covalency governs the intrinsic activity of Co-Mn spinel oxides for boosted peroxymonosulfate activation, *Angew. Chem. Int. Ed.* 60 (1) (2021) 274–280, <https://doi.org/10.1002/anie.v60.110.1002/anie.202010828>.
- [11] D.A. Armstrong, R.E. Huie, S. Lyman, W.H. Koppenol, G. Merényi, P. Neta, D.M. Stanbury, S. Steenken, P. Wardman, Standard electrode potentials involving radicals in aqueous solution: inorganic radicals (IUPAC Technical Report), *Pure Appl. Chem.* 87 (2015) 1139–1150. Doi: 10.1515/pac-2014-0502
- [12] A.K. Pikaev, V.I. Zolotarevskii, Pulse radiolysis of aqueous solutions of sulfuric acid, *Bull. Acad. Sci. USSR* 16 (1) (1967) 181–182, <https://doi.org/10.1007/BF00907128>.
- [13] X. Xia, F. Zhu, J. Li, H. Yang, L. Wei, Q. Li, J. Jiang, G. Zhang, Q. Zhao, A review study on sulfate-radical-based advanced oxidation processes for domestic/ industrial wastewater treatment: Degradation, efficiency, and mechanism, *Front. Chem.* 8 (2020), <https://doi.org/10.3389/fchem.2020.592056> 592056.
- [14] A. Romero, A. Santos, F. Vicente, C. González, Diuron abatement using activated persulfate: effect of pH, Fe(II) and oxidant dosage, *Chem. Eng. J.* 162 (1) (2010) 257–265, <https://doi.org/10.1016/j.cej.2010.05.044>.
- [15] E. Brillas, I. Sirés, M.A. Oturan, Electro-Fenton process and related electrochemical technologies based on Fenton's reaction chemistry, *Chem. Rev.* 109 (12) (2009) 6570–6631, <https://doi.org/10.1021/cr900136g>.
- [16] C.A. Martínez-Huitle, M.A. Rodrigo, I. Sirés, O. Scialdone, Single and coupled electrochemical processes and reactors for the abatement of organic water pollutants: A critical review, *Chem. Rev.* 115 (24) (2015) 13362–13407, <https://doi.org/10.1021/acs.chemrev.5b00361>.
- [17] A. Galia, S. Lanzalaco, M.A. Sabatino, C. Dispenza, O. Scialdone, I. Sirés, Crosslinking of poly(vinylpyrrolidone) activated by electrogenerated hydroxyl radicals: A first step towards a simple and cheap synthetic route of nanogel vectors, *Electrochim. Commun.* 62 (2016) 64–68, <https://doi.org/10.1016/j.jelecom.2015.12.005>.
- [18] R. Salazar, J. Gallardo-Arriaza, J. Vidal, C. Rivera-Vera, C. Toledo-Neira, M.A. Sandoval, L. Cornejo-Ponce, A. Thiam, Treatment of industrial textile wastewater by the solar photoelectro-Fenton process: Influence of solar radiation and applied current, *Solar Energy* 190 (2019) 82–91, <https://doi.org/10.1016/j.solener.2019.07.072>.
- [19] G. Daniel, Y. Zhang, S. Lanzalaco, F. Brombin, T. Kosmala, G. Granozzi, A. Wang, E. Brillas, I. Sirés, C. Durante, Chitosan-derived nitrogen-doped carbon electrocatalyst for a sustainable upgrade of oxygen reduction to hydrogen peroxide in UV-assisted electro-Fenton water treatment, *ACS Sustain. Chem. Eng.* 8 (38) (2020) 14425–14440, <https://doi.org/10.1021/acsschemeng.0c04294>.
- [20] D. Medeiros de Araújo, C. Sáez, P. Cañizares, M.A. Rodrigo, C.A. Martínez-Huitle, Improving the catalytic effect of peroxodisulfate and peroxodiphosphate electrochemically generated at diamond electrode by activation with light irradiation, *Chemosphere* 207 (2018) 774–780, <https://doi.org/10.1016/j.chemosphere.2018.05.121>.
- [21] K. Groenen-Serrano, A critical review on the electrochemical production and use of peroxo-compounds, *Curr. Opin. Electrochem.* 27 (2021) 100679, <https://doi.org/10.1016/j.coelec.2020.100679>.
- [22] O. Scialdone, A. Galia, C. Gattuso, S. Sabatino, B. Schiavo, Effect of air pressure on the electro-generation of H<sub>2</sub>O<sub>2</sub> and the abatement of organic pollutants in water by electro-Fenton process, *Electrochim. Acta* 182 (2015) 775–780, <https://doi.org/10.1016/j.electacta.2015.09.109>.
- [23] A. Thiam, I. Sirés, E. Brillas, Treatment of a mixture of food color additives (E122, E124 and E129) in different water matrices by UVA and solar photoelectro-Fenton, *Water Res.* 81 (2015) 178–187, <https://doi.org/10.1016/j.watres.2015.05.057>.
- [24] S. Cotillas, J. Llanos, P. Cañizares, D. Clematis, G. Cerisola, M.A. Rodrigo, M. Panizza, Removal of Procion Red MX-5B dye from wastewater by conductive-diamond electrochemical oxidation, *Electrochim. Acta* 263 263 (2018) 1–7, <https://doi.org/10.1016/j.electacta.2018.01.052>.
- [25] M. Panizza, A. Barbucci, R. Ricotti, G. Cerisola, Electrochemical degradation of methylene blue, *Sep. Purif. Technol.* 54 (3) (2007) 382–387, <https://doi.org/10.1016/j.seppur.2006.10.010>.
- [26] C. Liang, H.-W. Su, Identification of sulfate and hydroxyl radicals in thermally activated persulfate, *Ind. Eng. Chem. Res.* 48 (11) (2009) 5558–5562, <https://doi.org/10.1021/ie9002848>.
- [27] C.M. Dominguez, A. Romero, D. Lorenzo, A. Santos, Thermally activated persulfate for the chemical oxidation of chlorinated organic compounds in groundwater, *J. Environ. Manage.* 261 (2020) 110240, <https://doi.org/10.1016/j.jenvman.2020.110240>.
- [28] C. Telegang Chekem, S. Chiron, J.M. Mancaux, G. Plantard, V. Goetz, Thermal activation of persulfates for wastewater depollution on pilot scale solar equipment, *Solar Energy* 205 205 (2020) 372–379, <https://doi.org/10.1016/j.solener.2020.04.075>.
- [29] D.A. House, Kinetics and mechanism of oxidations by peroxydisulfate, *Chem. Rev.* 62 (3) (1962) 185–203, <https://doi.org/10.1021/cr60217a001>.
- [30] G.V. Buxton, T.N. Malone, G. Arthur Salmon, Reaction of SO<sub>4</sub><sup>•−</sup> with Fe<sup>2+</sup>, Mn<sup>2+</sup> and Cu<sup>2+</sup> in aqueous solution, *J. Chem. Soc., Faraday Trans.* 93 (1997) 2893–2897, <https://doi.org/10.1039/A701472D>.
- [31] S.A. Shafiee, J. Aarons, H.H. Hamzah, Review—Electroreduction of peroxodisulfate: A review of a complicated reaction, *J. Electrochem. Soc.* 165 (13) (2018) H785–H798, <https://doi.org/10.1149/2.116181jes>.
- [32] A. Jhones dos Santos, I. Sirés, E. Brillas, Removal of bisphenol A from acidic sulfate medium and urban wastewater using persulfate activated with electrogenerated Fe<sup>2+</sup>, *Chemosphere* 263 (2021) 128271, <https://doi.org/10.1016/j.chemosphere.2020.128271>.
- [33] Z. Sun, S. Li, H. Ding, Y. Zhu, X. Wang, H. Liu, Q. Zhang, C. Zhao, Electrochemical/Fe<sup>3+</sup>/peroxymonosulfate system for the degradation of Acid Orange 7 adsorbed on activated carbon fiber cathode, *Chemosphere* 241 (2020) 125125, <https://doi.org/10.1016/j.chemosphere.2019.125125>.
- [34] A.J. dos Santos, E. Brillas, P.L. Cabot, I. Sirés, Simultaneous persulfate activation by electrogenerated H<sub>2</sub>O<sub>2</sub> and anodic oxidation at a boron-doped diamond anode for the treatment of dye solutions, *Sci. Total Environ.* 747 (2020) 141541, <https://doi.org/10.1016/j.scitotenv.2020.141541>.
- [35] F.J. Recio, P. Herrasti, I. Sirés, A.N. Kulak, D.V. Bavykin, C. Ponce-de-León, F.C. Walsh, The preparation of PbO<sub>2</sub> coatings on reticulated vitreous carbon for the electro-oxidation of organic pollutants, *Electrochim. Acta* 56 (14) (2011) 5158–5165, <https://doi.org/10.1016/j.electacta.2011.03.054>.
- [36] G. Ramírez, F.J. Recio, P. Herrasti, C. Ponce-de-León, I. Sirés, Effect of RVC porosity on the performance of PbO<sub>2</sub> composite coatings with titanate nanotubes for the electrochemical oxidation of azo dyes, *Electrochim. Acta* 204 (2016) 9–17, <https://doi.org/10.1016/j.electacta.2016.04.054>.
- [37] J. Cai, T. Niu, P. Shi, G. Zhao, Boron-doped diamond for hydroxyl radical and sulfate radical anion electrogeneration, transformation, and voltage-free sustainable oxidation, *Small* 15 (48) (2019) 1900153, <https://doi.org/10.1002/sml.v15.4810.1002/sml.201900153>.
- [38] H. Song, L. Yan, Y. Wang, J. Jiang, J. Ma, C. Li, G. Wang, J. Gu, P. Liu, Electrochemically activated PMS and PDS: Radical oxidation versus nonradical oxidation, *Chem. Eng. J.* 391 (2020) 123560, <https://doi.org/10.1016/j.cej.2019.123560>.
- [39] D. Zhi, Y. Lin, L.I. Jiang, Y. Zhou, A. Huang, J. Yang, L. Luo, Remediation of persistent organic pollutants in aqueous systems by electrochemical activation of persulfates: A review, *J. Environ. Manage.* 260 (2020) 110125, <https://doi.org/10.1016/j.jenvman.2020.110125>.
- [40] W.-S. Chen, Y.-C. Jhou, C.-P. Huang, Mineralization of dinitrotoluenes in industrial wastewater by electro-activated persulfate oxidation, *Chem. Eng. J.* 252 (2014) 166–172, <https://doi.org/10.1016/j.cej.2014.05.033>.
- [41] W.-S. Chen, C.-P. Huang, Mineralization of aniline in aqueous solution by electrochemical activation of persulfate, *Chemosphere* 125 (2015) 175–181, <https://doi.org/10.1016/j.chemosphere.2014.12.053>.
- [42] J. Wu, H. Zhang, J. Qiu, Degradation of Acid Orange 7 in aqueous solution by a novel electro/Fe<sup>2+</sup>/peroxydisulfate process, *J. Hazard. Mater.* 215–216 (2012) 138–145, <https://doi.org/10.1016/j.jhazmat.2012.02.047>.
- [43] H. Zeng, S. Liu, B. Chai, D.I. Cao, Y. Wang, X.u. Zhao, Enhanced photoelectrocatalytic decomplexation of Cu-EDTA and Cu recovery by persulfate activated by UV and cathodic reduction, *Environ. Sci. Technol.* 50 (12) (2016) 6459–6466, <https://doi.org/10.1021/acs.est.6b0063210.1021/acs.est.6b00632.s001>.
- [44] C. Nie, Z. Ao, X. Duan, C. Wang, S. Wang, T. An, Degradation of aniline by electrochemical activation of peroxydisulfate at MWCNT cathode: The proofed



- concept of nonradical oxidation process, *Chemosphere* 206 (2018) 432–438, <https://doi.org/10.1016/j.chemosphere.2018.04.173>.
- [45] L.W. Matzek, M.J. Tipton, A.T. Farmer, A.D. Steen, K.E. Carter, Understanding electrochemically activated persulfate and its application to ciprofloxacin abatement, *Environ. Sci. Technol.* 52 (10) (2018) 5875–5883, <https://doi.org/10.1021/acs.est.8b00015>.
- [46] F.C. Walsh, L.F. Arenas, C. Ponce de León, G.W. Reade, I. Whyte, B.G. Mellor, The continued development of reticulated vitreous carbon as a versatile electrode material: Structure, properties and applications, *Electrochim. Acta* 215 (2016) 566–591, <https://doi.org/10.1016/j.electacta.2016.08.103>.
- [47] L.F. Castañeda, F.C. Walsh, J.L. Nava, C. Ponce de León, Graphite felt as a versatile electrode material: Properties, reaction environment, performance and applications, *Electrochim. Acta* 258 (2017) 1115–1139, <https://doi.org/10.1016/j.electacta.2017.11.165>.
- [48] I. Sirés, C.T.J. Low, C. Ponce-de-León, F.C. Walsh, The deposition of nanostructured  $\beta$ -PbO<sub>2</sub> coatings from aqueous methanesulfonic acid for the electrochemical oxidation of organic pollutants, *Electrochem. Commun.* 12 (2010) 70–74, <https://doi.org/10.1016/j.elecom.2009.10.038>.
- [49] K. Hou, Z. Pi, F. Yao, B.o. Wu, L.i. He, X. Li, D. Wang, H. Dong, Q.i. Yang, A critical review on the mechanisms of persulfate activation by iron-based materials: Clarifying some ambiguity and controversies, *Chem. Eng. J.* 407 (2021) 127078, <https://doi.org/10.1016/j.cej.2020.127078>.
- [50] J. Liu, J. Zhou, Z. Ding, Z. Zhao, X. Xu, Z. Fang, Z. Fang, Ultrasound irradiation enhanced heterogeneous activation of peroxymonosulfate with Fe<sub>3</sub>O<sub>4</sub> for degradation of azo dye, *Ultrason. Sonochem.* 34 (2017) 953–959, <https://doi.org/10.1016/j.ultsonch.2016.08.005>.
- [51] Z. Dong, Q. Zhang, B.-Y. Chen, J. Hong, Oxidation of bisphenol A by persulfate via Fe<sub>3</sub>O<sub>4</sub>- $\alpha$ -MnO<sub>2</sub> nanoflower-like catalyst: Mechanism and efficiency, *Chem. Eng. J.* 357 (2019) 337–347, <https://doi.org/10.1016/j.cej.2018.09.179>.
- [52] Z. Pi, X. Li, D. Wang, Q. Xu, Z. Tao, X. Huang, F. Yao, Y. Wu, L. He, Q. Yang, Persulfate activation by oxidation biochar supported magnetite particles for tetracycline removal: Performance and degradation pathway, *J. Cleaner Prod.* 235 (2019) 1103–1115, <https://doi.org/10.1016/j.jclepro.2019.07.037>.
- [53] H. Lin, H. Zhang, L. Hou, Degradation of C. I. Acid Orange 7 in aqueous solution by a novel electro/Fe<sub>3</sub>O<sub>4</sub>/PDS process, *J. Hazard. Mater.* 276 (2014) 182–191, <https://doi.org/10.1016/j.jhazmat.2014.05.021>.
- [54] I. Lozano, C. López, N. Menendez, N. Casillas, P. Herrasti, Design, construction and evaluation of a 3D printed electrochemical flow cell for the synthesis of magnetite nanoparticles, *J. Electrochem. Soc.* 165 (11) (2018) H688–H697, <https://doi.org/10.1149/2.1401810jes>.
- [55] R.A. Brand, Improving the validity of hyperfine field distributions from magnetic alloys, *Nucl. Instruments Methods Phys. Res. Sect. B: Beam Interact. with Mater. Atoms* 28 (3) (1987) 398–416, [https://doi.org/10.1016/0168-583X\(87\)90182-0](https://doi.org/10.1016/0168-583X(87)90182-0).
- [56] F. Alcaide, G. Álvarez, D.R.V. Guelfi, E. Brillas, I. Sirés, A stable CoSP/MWCNTs air-diffusion cathode for the photoelectro-Fenton degradation of organic pollutants at pre-pilot scale, *Chem. Eng. J.* 379 (2020) 122417, <https://doi.org/10.1016/j.cej.2019.122417>.
- [57] K. Woo, J. Hong, S. Choi, H.-W. Lee, J.-P. Ahn, C.S. Kim, S.W. Lee, Easy synthesis and magnetic properties of iron oxide nanoparticles, *Chem. Mater.* 16 (14) (2004) 2814–2818, <https://doi.org/10.1021/cm049552x>.
- [58] J.J.P. Roberts, J.A. Westgard, L.M. Cooper, R.W. Murray, Solution voltammetry of 4 nm magnetite ion oxide nanoparticles, *J. Am. Chem. Soc.* 136 (2014) 10783–10789, <https://doi.org/10.1021/ja505562p>.
- [59] H. Zhu, S. Zhang, Y.-X. Huang, L. Wu, S. Sun, Monodisperse M<sub>x</sub>Fe<sub>3-x</sub>O<sub>4</sub> (M = Fe, Cu Co, Mn) nanoparticles and their electrocatalysis for oxygen reduction reaction, *Nano Lett.* 13 (6) (2013) 2947–2951, <https://doi.org/10.1021/nl401325u>.
- [60] J.H. Zagal, F.J. Recio, C.A. Gutierrez, C. Zúñiga, M.A. Páez, C.A. Caro, Towards a unified way of comparing the electrocatalytic activity MN<sub>x</sub> macrocyclic metal catalysts for O<sub>2</sub> reduction on the basis of the reversible potential of the reaction, *Electrochem. Commun.* 41 (2014) 24–26, <https://doi.org/10.1016/j.elecom.2014.01.009>.
- [61] R. Venegas, K. Muñoz-Becerra, C. Candia-Onfray, J.F. Marco, J.H. Zagal, F.J. Recio, Experimental reactivity descriptors of M-N-C catalysts for the oxygen reduction reaction, *Electrochim. Acta* 332 (2020) 135340, <https://doi.org/10.1016/j.electacta.2019.135340>.
- [62] Y. Zhang, G. Daniel, S. Lanzalaco, A.A. Isse, A. Facchin, A. Wang, E. Brillas, C. Durante, I. Sirés, H<sub>2</sub>O<sub>2</sub> production at gas-diffusion cathodes made from agarose-derived carbons with different textural properties for acetolol degradation in chloride media, *J. Hazard. Mater.* 423 (2022) 127005, <https://doi.org/10.1016/j.jhazmat.2021.127005>.
- [63] H. Luo, Y. Cheng, Y. Zeng, K. Luo, D. He, X. Pan, Rapid removal of organic micropollutants by heterogeneous peroxymonosulfate catalysis over a wide pH range: Performance, mechanism and economic analysis, *Sep. Purif. Technol.* 248 (2020) 117023, <https://doi.org/10.1016/j.seppur.2020.117023>.
- [64] H. Paudyal, B. Pangeni, K. Inoue, H. Kawakita, K. Ohto, H. Harada, S. Alam, Adsorptive removal of fluoride from aqueous solution using orange waste loaded with multi-valent metal ions, *J. Hazard. Mater.* 192 (2) (2011) 676–682, <https://doi.org/10.1016/j.jhazmat.2011.05.070>.
- [65] O. Duman, S. Tunç, T.G. Polat, B.K. Bozoğlan, Synthesis of magnetic oxidized multiwalled carbon nanotube- $\kappa$ -carrageenan-Fe<sub>3</sub>O<sub>4</sub> nanocomposite adsorbent and its application in cationic Methylene Blue dye adsorption, *Carbohydr. Polym.* 147 (2016) 79–88, <https://doi.org/10.1016/j.carbpol.2016.03.099>.
- [66] A.S. Helal, E. Mazario, A. Mayoral, P. Decorse, R. Losno, C. Lion, S. Ammar, M. Hémadi, Highly efficient and selective extraction of uranium from aqueous solution using a magnetic device: succinyl- $\beta$ -cyclodextrin-APTES@maghemite nanoparticles, *Environ. Sci. Nano.* 5 (1) (2018) 158–168, <https://doi.org/10.1039/C7EN00902J>.
- [67] F.L. Rivera, F.J. Palomares, P. Herrasti, E. Mazario, Improvement in heavy metal removal from wastewater using an external magnetic inductor, *Nanomaterials* 9 (2019) 1508, <https://doi.org/10.3390/nano9111508>.
- [68] Y. Li, A.R. Zimmerman, F. He, J. Chen, L. Han, H. Chen, X. Hu, B. Gao, Solvent-free synthesis of magnetic biochar and activated carbon through ball-mill extrusion with Fe<sub>3</sub>O<sub>4</sub> nanoparticles for enhancing adsorption of methylene blue, *Sci. Total Environ.* 722 (2020) 137972, <https://doi.org/10.1016/j.scitotenv.2020.137972>.
- [69] F.L. Rivera, F.J. Recio, F.J. Palomares, J. Sánchez-Marcos, N. Menéndez, E. Mazario, P. Herrasti, Fenton-like degradation enhancement of methylene blue dye with magnetic heating induction, *J. Electroanal. Chem.* 879 (2020) 114773, <https://doi.org/10.1016/j.jelechem.2020.114773>.
- [70] C.-M. Hung, C.-W. Chen, Y.-Z. Zhuang, C.-D. Dong, Fe<sub>3</sub>O<sub>4</sub> magnetic nanoparticles: Characterization and performance exemplified by the degradation of Methylene Blue in the presence of persulfate, *J. Adv. Oxid. Technol.* 19 (2016) 43–51, <https://doi.org/10.1515/jaots-2016-0105>.
- [71] A. Ghauch, A.M. Tuqan, N. Kibbi, S. Geryes, Methylene blue discoloration by heated persulfate in aqueous solution, *Chem. Eng. J.* 213 (2012) 259–271, <https://doi.org/10.1016/j.cej.2012.09.122>.